JOURNAL OF MATERIALS SCIENCE **36** (2001) 4493–4501

Ageing behaviour of zirconia stabilised by yttria and manganese oxide

C. C. APPEL,* N. BONANOS, A. HORSEWELL,† S. LINDEROTH
Materials Research Department, Risø National Laboratory, DK-4000 Roskilde, Denmark
E-mail: CCA@topsoe.dk

The effect of Mn on the structure, lattice parameter and conductivity has been investigated for near-cubic YSZ with an yttrium content slightly under 8 mol% Y_2O_3. The structure and chemistry of the material were studied both as sintered, and also after prolonged heat treatments at 850 and 1000°C, using x-ray diffraction, electron microscopy, impedance spectroscopy and d.c. conductivity measurements. In the latter case, the measurements were made in-situ during ageing. At 1000°C and for Mn additions above about 2 mol% YSZ is found to be stabilised as the cubic structure, and thereby the conductivity is also stabilised. However, at all temperatures studied, the presence of Mn considerably reduces the ionic conductivity of YSZ.

1. Introduction

Cubic zirconia stabilised with yttria (YSZ) is the preferred electrolyte in current solid oxide fuel cells (SOFCs) (see for example [1]). The oxide ion conductivity of YSZ strongly depends on the yttrium content and temperature. In the temperature interval 850–1000°C, the highest conductivity is obtained for compositions in the region of 8 mol% Y_2O_3 [2]. As illustrated in Fig. 1 (adapted from [3]), parts of the ZrO_2-Y_2O_3 phase diagram are in dispute, especially close to the composition 8 mol% Y_2O_3 (8YSZ).‡ At temperatures typical of sintering e.g. 1350–1550°C, the system is in the fully cubic phase field, while from operating temperatures of 1000°C down to about 500°C, it is uncertain whether the equilibrium is in the cubic or the tetragonal + cubic phase field (cf. Fig. 1). The temperature at which the equilibrium phase composition shifts from fully cubic to a mixture of cubic and tetragonal is not known with certainty.

It is well established that the conductivity of 8YSZ decreases during ageing at 1000°C [2]; this is understood to be mainly due to the cubic to tetragonal phase transformation. The exact location of the conductivity maximum depends on the ageing condition of the sample. For YSZ to have a satisfactory oxide ion conductivity and maintain it during long term operation, the yttrium content should be just high enough to stabilise the cubic phase at the operating temperature. Thus, as-prepared 7.7YSZ has a higher oxide ion conductivity than 8.5YSZ, but after 80 hours of ageing at 1000°C, the situation is reversed [4]. A slight decrease in the conductivity of 9.5YSZ reported in the same study has been attributed to electrode effects. Relevance to SOFC operation demands a prolonged ageing study, i.e. in excess of 1000 h, and where possible, a technique that is insensitive to changes in the electrode impedance, namely four terminal resistance measurements.

Manganese is soluble in YSZ, with a solubility limit between 5 mol% at 1000°C and 15 mol% at 1500°C [5]. 7.5YSZ with 2 mol% or more Mn, sintered at 1400°C, retained the cubic form [6] and Mn was shown to prevent formation of the tetragonal phase [7]. Mn dissolved in 9.5YSZ is a mixture of Mn^{2+} and Mn^{3+} [8]. An increasing Mn-content in 7.5YSZ results in a decrease in the coordination number of the cation sites occupied by Mn-ions due to the association of the Mn-ions with the increasing concentration of oxide vacancies [7].

$LaMnO_3$-based perovskites are commonly used as cathode materials in SOFCs and it is well known that Mn diffuses from the cathode into the electrolyte [9]. Therefore, it would be advantageous if Mn could be used to enhance the stability of the cubic phase and thus prevent degradation of the oxide ion conductivity with time. The present work is an investigation of the effect of manganese on the structure, initial oxide ion conductivity and ageing behaviour of 8YSZ. The materials used for this study were in the form of sintered tape of the type prepared for planar SOFCs.

2. Sample preparation and experimental techniques

The nominal compositions and names of the samples studied are given in Table I. All except one were prepared using 7.9YSZ powder from Tosoh with the composition:§ 85.76 weight% ZrO_2, 13.47 weight%

*Present Address: Haldor Topsøe A/S Nymøllevej 55, DK-2800 Lyngby, Denmark.
†Present Address: Technical University of Denmark, DK-2800 Lyngby, Denmark.
‡In the following, compositions are described by the notation *x*YSZ where *x* is the Y_2O_3-content in mol% i.e. 8 mol% Y_2O_3 is shortened to 8YSZ.
§Based on analysis supplied by Tosoh.

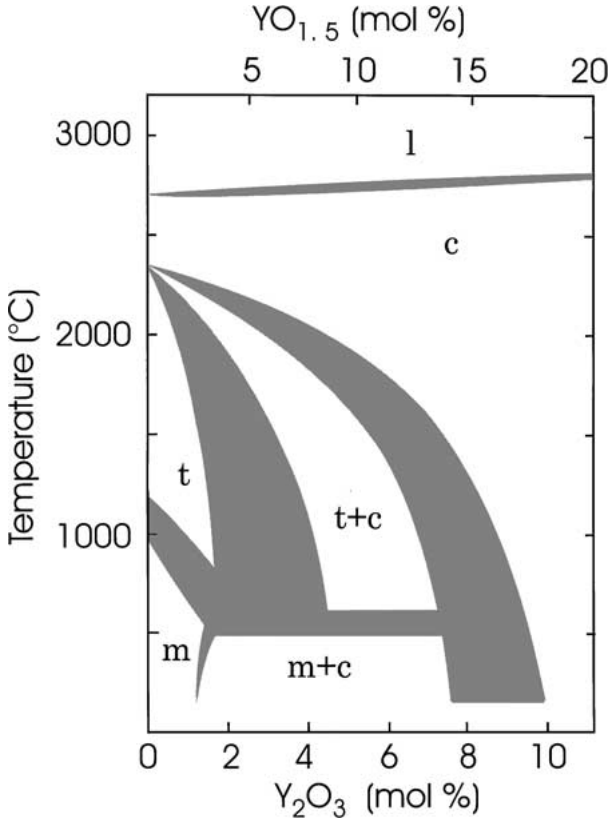

Figure 1 ZrO_2-Y_2O_3 phase diagram for the ZrO_2 rich region, showing the uncertainty regarding the borders between the cubic to tetragonal phase fields. The shaded areas indicate the range of phase boundary lines reported in the literature. Adapted from Yoshimura [3].

(≈7.89 mol%) Y_2O_3 and <1 weight% other oxides. One sample was prepared from 86.48 weight% ZrO_2, 12.78 weight% (≈7.46 mol%) Y_2O_3 and <1 weight% of other oxides (≈7.5YSZ). Portions of the 7.9YSZ powder were mixed with $MnCO_3$ by ball milling using zirconia balls in a plastic container. The ball milled powders were tape cast following in-house established techniques [10] and sintered at 1350°C for 8 hours, giving tapes of thickness circa 160 μm. During sintering, the $MnCO_3$ was converted to oxide, which dissolved in the YSZ. The samples are named according to their yttria content in mol% and, where appropriate, their Mn content in atomic% of metal ions.

Electrical characterisation was performed using ac and dc conductivity measurements. Impedance spectroscopy was used to resolve the grain interior and grain boundary resistance components. Impedance spectra were obtained on 7.6 mm diameter discs of tape cast material (Fig. 2a) with platinum paste electrodes, in

TABLE I The nominal cation composition of the examined samples. The oxygen content was not used in the calculation, because the oxidation state of Mn is not known exactly

Sample	Zr (atomic% of cations)	Y (atomic% of cations)	Mn (atomic% of cations)
7.5YSZ	86.1	13.9	0
7.9YSZ	85.4	14.6	0
7.9YSZ1MN	84.5	14.5	1.0
7.9YSZ2Mn	83.7	14.4	2.0
7.9YSZ5Mn	81.1	13.9	5.0

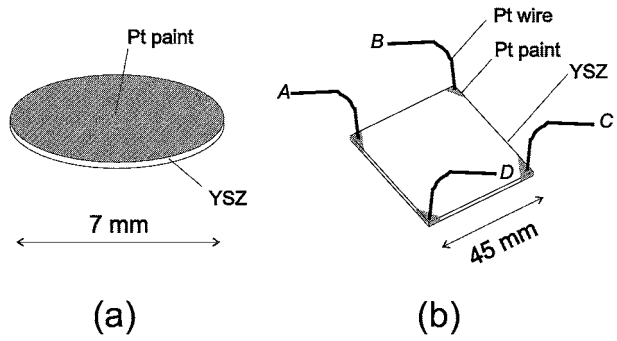

Figure 2 Sample geometries used in (a) transverse conductivity measurements using impedance spectroscopy [15] and (b) In-plane dc measurement using the van der Pauw technique [12].

air, in the temperature range 300 to 1000°C, using a *Solartron 1260* impedance analyser. The combined error of contact and uncompensated lead resistance was estimated to be of the order of 0.1 Ω. At 800°C, where the resistance of a typical tape sample falls to about 1 Ω, this error becomes significant, therefore, only impedance data below 800°C are reported here. The impedance data were analysed using the software *Equivcrt* [11]. For the conductivity ageing studies, which were performed above 800°C, the four-probe van der Pauw technique was used [12], as implemented by Poulsen *et al.* [13]. Square tape cast samples of dimensions 45 × 45 mm had platinum leads attached to their corners. Measurements were made by imposing a current via two adjacent probes and measuring the voltage at the opposite ones, in two settings, (i) as shown in Fig. 2b and (ii) with the connections rotated in the sense A→B→C→D. In each case, the four-terminal resistances, R_{ABDC} and R_{BCAD} were calculated from the slope of the voltage against current. The conductivity was calculated via the formula given by van der Pauw:

$$\sigma = \left(\frac{\pi \cdot d}{\ln 2} \cdot \frac{R_{ABDC} + R_{BCAD}}{2} \cdot f \right)^{-1}$$

where d is the sample thickness and f is a dimensionless factor dependant on the disparity between R_{ABDC} and R_{BCAD}. According to an approximation of f given by van der Pauw [12], if the two resistances differ by less than 30% then $0.99 \leq f \leq 1$. As this condition was true for all the present measurements, errors in the calculation of f are insignificant.

X-ray diffraction (XRD) was used to obtain the cubic lattice parameter of the sintered material. The measurements were performed on powders prepared from crushed tapes, on a STOE 2-theta diffractometer, using an internal NBS silicon standard. Cu K_α was used with a bent Ge monochromatic and a position sensitive detector. The measurements were made in transmission mode.

Scanning electron microscopy (SEM) characterisations were carried out in a low vacuum SEM (LVSEM), JEOL LV5310, operated in low vacuum mode; thus coating with an electron conductive layer was avoided.

The transmission electron microscope (TEM) used was a JEOL 2000FX equipped with energy dispersive

X-ray spectrometry (EDS). Specimens for the TEM examinations were polished and thinned to electron transparency by sputtering with ≈5 kV Ar-ions at low angles using a GATAN precision ion polisher (PIPS). The specimens prepared for TEM were coated with carbon, to prevent charging during observation.

3. Results

3.1. Electrical characterisation

Typically, impedance spectra obtained for zirconia ceramics contain grain interior, grain boundary and electrode impedance arcs, see for example [14, 15]. Fig. 3 shows spectra for the 7.9YSZ, 7.9YSZ2Mn and 7.9YSZ5Mn samples at 300°C. The first two spectra show well-defined grain interior and grain boundary relaxations, from which the resistances, respectively r_{gi}, r_{gb}, could be readily estimated by fitting. In the third spectrum, the grain boundary resistance was too low to be resolved. The grain interior resistivity increases with addition of Mn.

Fig. 4 shows Arrhenius plots of the grain interior and grain boundary components of resistivity for the above samples. Note that grain interior and grain boundary components can only be resolved over that part of the temperature range where the grain boundary relaxation frequency falls within the range of the impedance analyser, namely below 500°C. On the other hand, the sum of the two contributions, $r_{gi} + r_{gb}$, can be evaluated at all the temperatures used. At the low Mn doping levels employed here, the conductivity is expected to be predominantly ionic.

Fig. 5 shows the total conductivities, i.e. $(r_{gi} + r_{gb})^{-1}$, obtained by impedance spectroscopy at 560 to 800°C, together with the initial values measured by dc at 850 and 1000°C. In the latter data set, obtained as part of the ageing study, each data point corresponds to a different sample. The sample measured by dc at 850°C (7.5YSZ) had a slightly lower yttrium content than the others and this may partly explain why its conductivity is slightly higher than expected. There is some discrepancy between the dc data as a whole and the extrapolated ac data, which is systematic and cannot be attributed to variations among samples. Nevertheless, this does not contradict the overall conclusion that manganese doping reduces the conductivity of YSZ.

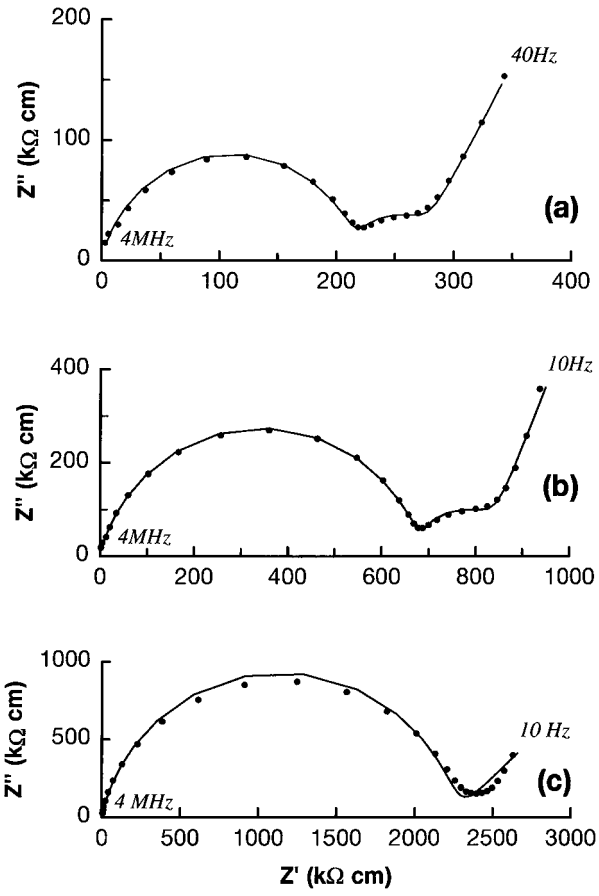

Figure 3 Impedance spectra obtained in air at 300°C, with (a) 7.9YSZ, (b) 7.9YSZ2Mn and (c) 7.9YSZ5Mn. In (a) and (b) the grain interior and grain boundary relaxations can be resolved by fitting. In (c) the grain boundary resistance was too low to be resolved.

3.2. Degradation of oxide ion conductivity

The conductivity of the samples held at 1000°C over an ageing period of 2000 hours in air is shown in Fig. 6a. The 7.9YSZ sample shows the highest degradation rate. The addition of manganese reduces the degradation rate as well as the initial conductivity; in fact, the conductivity of the 7.9YSZ5Mn sample, rather than decreasing, increases very slowly with ageing. Fig. 6b shows the results of a similar ageing study at 850°C for a period of 3000 hours (using fresh samples, one of which was 7.5YSZ). In this case, the effect of manganese is to depress the whole conductivity-time curve and to reduce, but not eliminate, the degradation of conductivity. The conductivities at the start of ageing and after specified times are given in Table II. The data for the non-aged samples correspond to the discrete data points in Fig. 5.

3.3. Structural characterisation

Fig. 7 shows the lattice parameters for as-prepared and heat treated samples with 0, 2 and 5% Mn. The lattice parameters decrease with increasing Mn content as previously reported by Appel [6]. During prolonged heat treatment at 1000°C the lattice parameters increase (Fig. 7). The increase in lattice parameter after 2000 hours at 1000°C is greater for 7.9YSZ and 7.9YSZ2Mn than for 7.9YSZ5Mn. This effect

TABLE II Time dependence of oxide ion conductivity for the tapes at 850 and 1000°C. The data were interpolated using fourth degree polynomial curves

	$\Delta\sigma$ ($t=0$) (ms/cm)		$\Delta\sigma$ (%) at 1000 h		$\Delta\sigma$ (%) at 2000 h		$\Delta\sigma$ (%) at 3000 h
Sample	850°C	1000°C	850°C	1000°C	850°C	1000°C	850°C
7.5YSZ	80	–	−12.7	–	−19.1	–	−23.2
7.9YSZ	–	192	–	−24.1	–	−33.4	–
7.9YSZ1Mn	65	151	−10.6	−24.0	−14.4	−35.8	−18.4
7.9YSZ2Mn	51	144	−8.9	−12.0	−11.8	−29.8	−15.6
7.9YSZ5Mn	33	111	−8.7	+1.7	−13.7	+1.8	−19.2

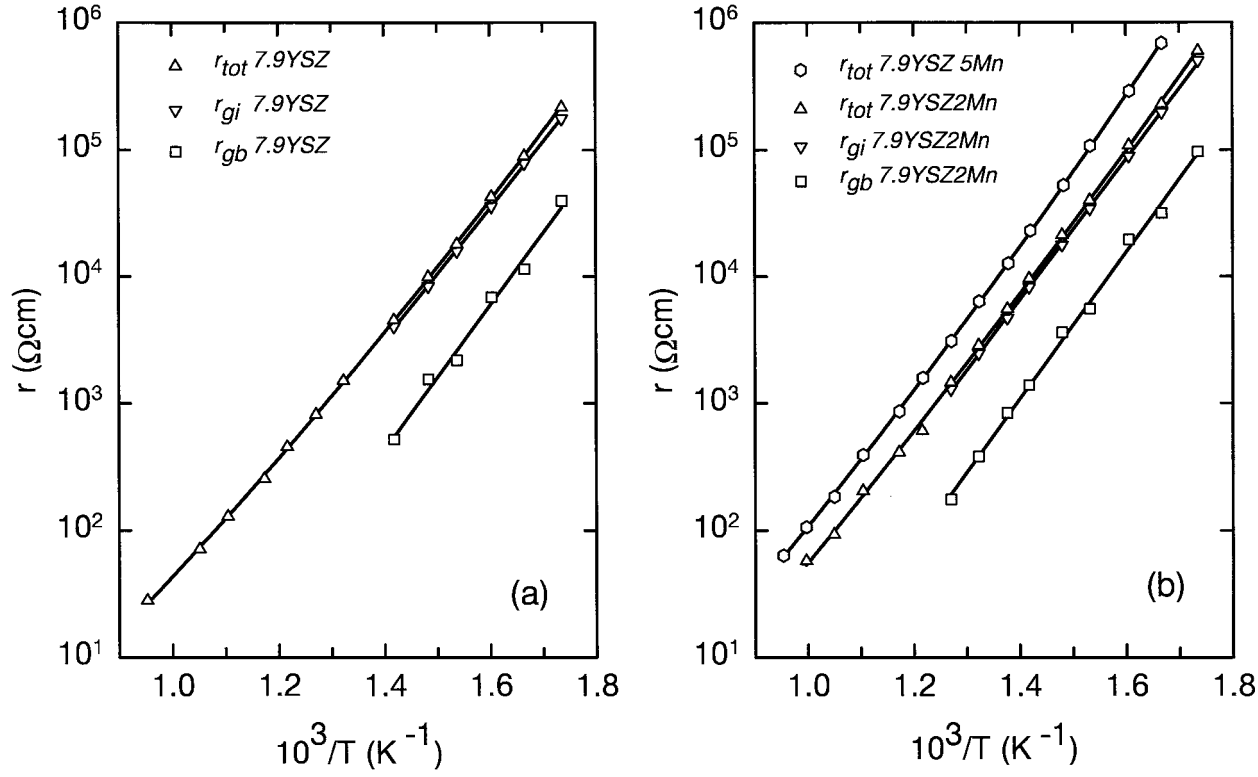

Figure 4 Arrhenius plots of the grain interior and grain boundary components of resistivity for the samples used in Fig. 3. The two components can be resolved at temperatures below 500°C. Their sum can be evaluated over the whole temperature range studied. (a) 7.9YSZ without Mn (b) 7.9YSZ2Mn and 7.9YSZ5Mn. In case of 7.9YSZ5Mn r_{gb} could not be resolved.

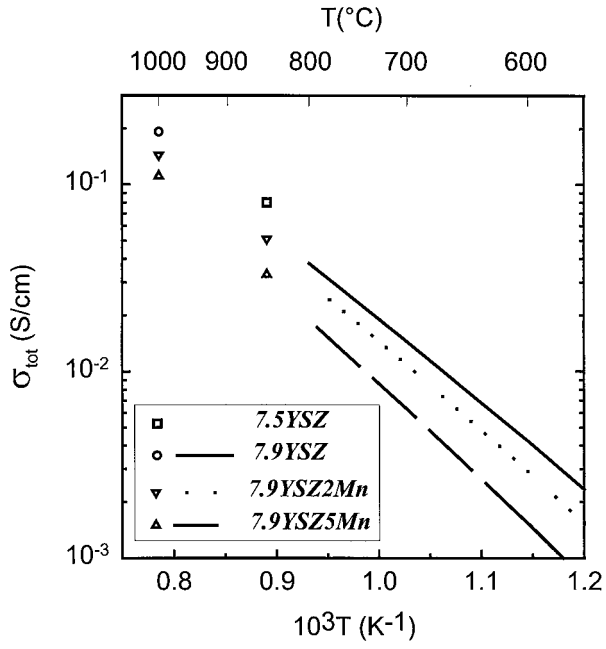

Figure 5 Total conductivities obtained by impedance spectroscopy (lines) and four point dc (discrete points). Note that each dc measurement was made on a different sample. The dc data are the conductivities obtained at the start of the ageing study.

on the lattice parameter is, in part, reversed by a heat treatment at 1350°C for 8 hours.

The surfaces of the as-prepared tapes were examined in the LVSEM to study differences in grain size among the various samples (Fig. 8a–c). The grain size of 7.9YSZ (Fig. 8a) varied between 1 and 2 μm. The grain size of 7.9YSZ2Mn (Fig. 8b) was 2 to 4 μm and the pores were larger than in the pure 7.9YSZ. With 7.9YSZ5Mn (Fig. 8c) up to 6 μm large grains were observed and pores were seen to be slightly larger than in 7.9YSZ2Mn. Ageing of 7.9YSZ2Mn at 1000°C for 2000 hours did not result in any observable grain growth.

The as-sintered samples were observed by TEM to be homogeneous. Mn was well distributed in solid solution in the grains. No amorphous grain boundary phases were observed in the as-prepared, sintered samples.

Selected area diffraction patterns (SADPs) obtained in the TEM were used to determine changes in the crystalline structure of the 7.9YSZ and its Mn-doped counterparts and to follow the structural changes occurring during ageing. No major changes in the SADPs were observed during the first 1000 hours of ageing. Fig. 9a–f shows SADPs taken along the [011]- and [112]-directions, respectively, of samples aged for 1000 hours. SADPs of the as-prepared samples [7] were substantially the same. In these diffraction patterns, the brightest spots are due to an fcc phase, namely cubic YSZ. In the cubic [011]-direction of 7.9YSZ and 7.9YSZ2Mn (Fig. 9a,b) weak spots are seen at {100} and {011} positions, which are forbidden for the fcc structure. These diffraction spots are slightly weaker for 7.9YSZ2Mn than for 7.9YSZ and are almost absent for 7.9YSZ5Mn (Fig. 9c). In the [112]-direction, the forbidden spots for the fcc structure are also seen on {011}-positions for 7.9YSZ (Fig. 9a) and 7.9YSZ2Mn (Fig. 9b). These forbidden spots are absent in 7.9YSZ5Mn (Fig. 9c), but instead, rings are seen in the diffuse background along the [131]-directions (not shown). Diffuse spots are also observed in the

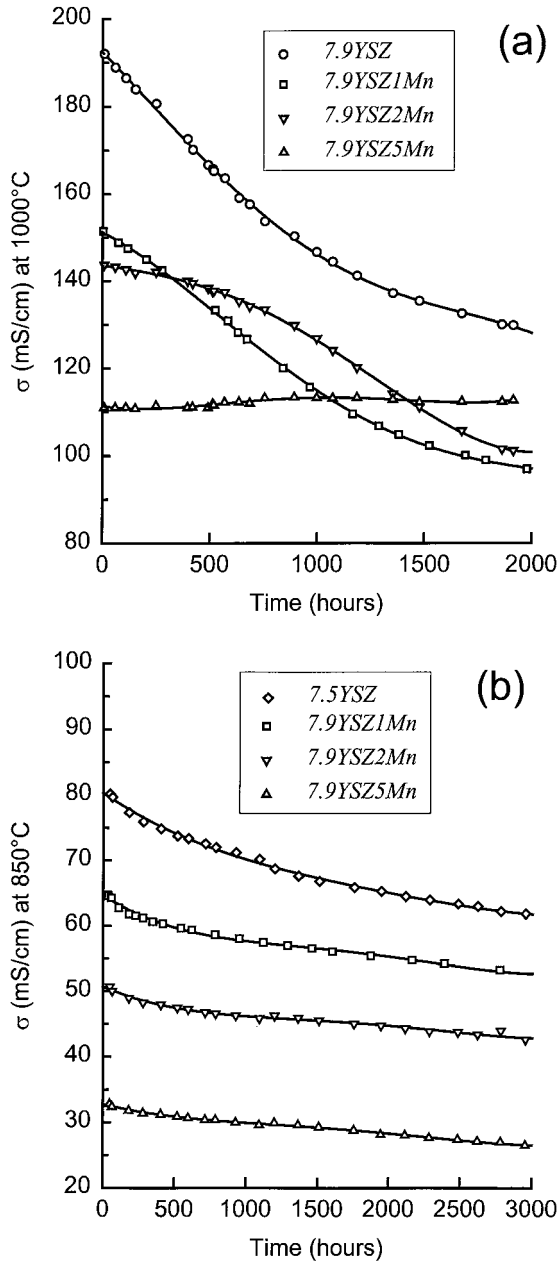

Figure 6 Long term conductivity study of samples of varying Mn-content at (a) 1000°C (b) 850°C.

[112]-direction of 7.9YSZ5Mn (Fig. 9f). TEM images of the as-prepared specimens and specimens aged for 1000 hours at 1000°C may show a characteristic mottled appearance. This mottling occurs only when a particular grain is tilted into a strong diffraction condition and is, therefore, associated with the appearance of forbidden spots in the diffraction patterns when the crystal is aligned close to a simple crystallographic direction.

Ageing for 2000 hours at 1000°C produced observable effects on the structure of 7.9YSZ2Mn. The forbidden diffraction spots are no longer observed in SADPs from the centres of grains (Fig. 10a); however, when an area close to the grain boundary is examined, the forbidden spots appear (Fig. 10b). Dark field imaging, where one of the forbidden diffraction spots is used to generate an image, reveals that the extra spots are produced by a concentration of crystallites in the grain boundary region (Fig. 11); the width of this region is 50–100 nm.

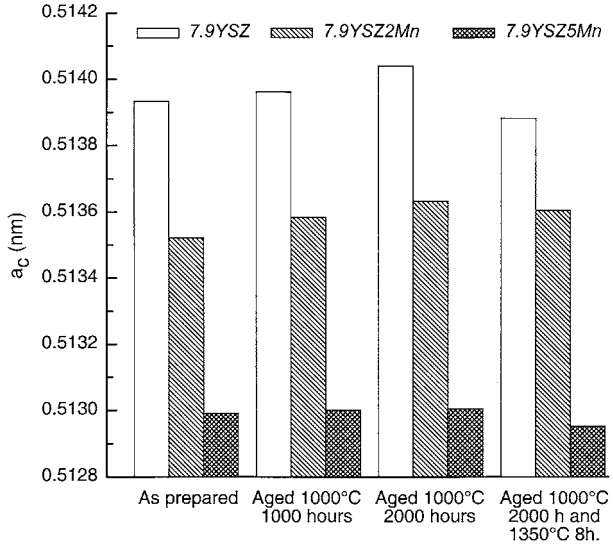

Figure 7 Lattice parameters for as-prepared and heat treated samples with 0, 2 and 5% Mn. The lattice parameters decrease with increasing Mn content and increase during prolonged heat treatment at 1000°C. This effect is in part, reversed by a heat treatment at 1350°C for 8 hours.

EDS-analyses of 7.9YSZ2Mn aged for 2000 hours in the centre of the grains and in the grain boundary regions show a reduced Mn-content in the region where these crystallites occur (Fig. 12). In this figure, the depletion of Mn is revealed by the high Y_2O_3/Mn_3O_4 ratio in the grain boundary regions, as compared to the grain centres. Note that the Y_2O_3/ZrO_2-ratio is the same in the grain boundary regions and in the grains.

4. Discussion

The decrease in lattice parameter with increasing Mn content in 7.9YSZ (cf. Fig. 7) shows that Mn goes into solid solution, as expected from Kawada *et al.* [5] and Appel [6]. The change in lattice parameter upon prolonged heat treatment at 1000°C can be explained by the transformation of some cubic YSZ to the tetragonal phase. The tetragonal phase will contain less than the average amount of yttrium, meaning that the remaining cubic phase will become richer in yttrium content. This increase in yttrium content of the cubic phase will result in an increase of the cubic lattice parameter [16–18]. The tetragonal phase is not found in the x-ray diffraction patterns, primarily because it generates broad diffraction peaks due to the small particle size of these regions. The smaller change for the 7.9YSZ5Mn sample compared to the samples containing less Mn is indicative of a stabilisation effect of the Mn on the cubic structure. The 1350°C treatment following the prolonged 1000°C ageing treatment resulted in a partial reversal of the lattice parameter changes due to a transformation of the tetragonal phase to cubic and redistribution of yttrium.

The addition of Mn caused formation of larger grains than in the pure 7.9YSZ as observed by SEM (cf. Fig. 8). This is in accordance with earlier observations of grain growth in YSZ when exposed to Mn-vapour [6].

Addition of Mn to 7.9YSZ causes a decrease in oxygen ion conductivity (cf. Table II). However, some advantage is gained from the addition of Mn because

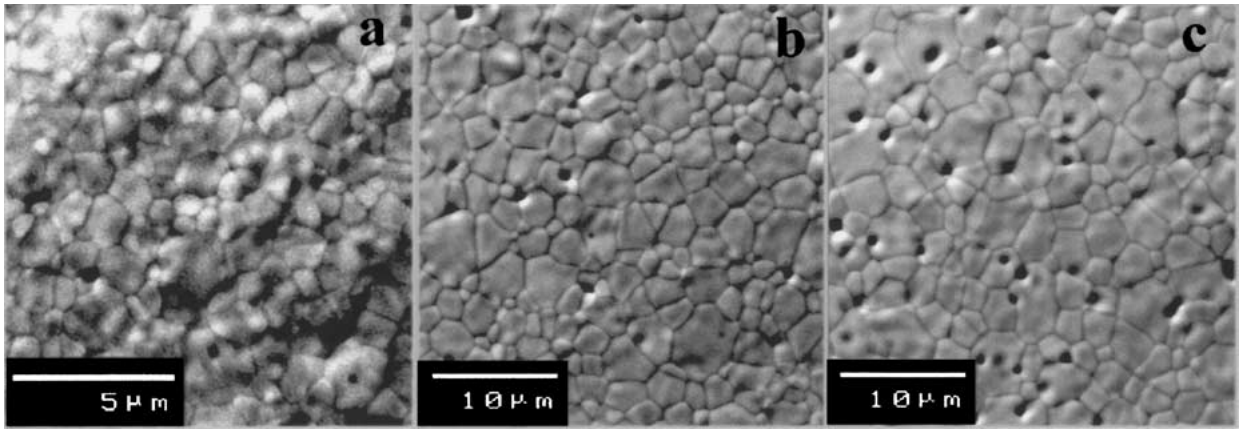

Figure 8 Scanning electron micrographs of surfaces of as-prepared tapes, obtained by LVSEM. (a) 7.9YSZ, (b) 7.9YSZ2Mn and (c) 7.9YSZ5Mn as prepared. Note that the scale bar of (a) is different from that in (b) and (c).

5 mol% Mn in 7.9YSZ prevents degradation of the conductivity during ageing. Badwal [2] showed that about 10 mol% Y_2O_3 is needed in zirconia to prevent degradation of the conductivity during ageing at 1000°C.

The electrical behaviour during ageing of the Mn-doped 7.9YSZ may be considered in terms of the structure. According to the 2-component phase diagram (ZrO_2-Y_2O_3) (see Fig. 1) 7.9YSZ is close to the phase boundary for fully stabilised cubic at the sintering temperature (1350°C), but at the ageing temperatures (1000 and 850°C) it may lie within the two-phase (tetragonal + cubic) field. SADPs of as-prepared 7.9YSZ show strong diffraction spots from cubic zirconia with Fm3m symmetry. Also, weak spots at positions which are forbidden for that symmetry, show phases which have a lower symmetry. The mottled appearance is caused by diffraction contrast from crystallites of this low symmetry phase. Very little contrast is expected from strain fields between the crystallites and the cubic matrix, since the tetragonal splitting is small.

The observation of symmetry lower than cubic Fm3m in 7.9YSZ is consistent with earlier observations in zirconia doped with similar amounts of Y_2O_3 [19, 20]. Zhou *et al*. [19] examined fully stabilised zirconia, i.e. doped with 14 mol% Y_2O_3 and observed no forbidden spots in the SADPs. In our SADPs, the forbidden spots are strongest for 7.9YSZ and are found to decrease with increasing Mn content. In 7.9YSZ5Mn the forbidden spots are no longer observed. This confirms the role of Mn in stabilising the cubic phase previously reported [7]. The existence of a fully stabilised cubic phase in 7.9YSZ5Mn at 1000°C is also confirmed by the ageing experiments, which show no degradation in the oxide ion conductivity at this temperature. A similar stability in conductivity with ageing is observed for 10YSZ, which is understood to be due to fully stabilised cubic zirconia [2].

7.9YSZ1Mn has a lower initial oxide ion conductivity than pure 7.9YSZ. However, the decrease in conductivity upon ageing is nearly the same for the two samples (Fig. 4) and the two curves remain offset by the same amount throughout the period of ageing. The SADPs showed the presence of a phase with a lower symmetry than that of Fm3m and the XRD of the as-prepared and aged 7.9YSZ showed changes in lattice parameter during ageing. This shows that some diffusion of cations may occur during the ageing. This is in accordance with earlier suggestions by Badwal [2] that ZrO_2 with less than 8–9 mol% M_2O_3 (M is a trivalent cation) decomposes by diffusion of yttrium into a tetragonal and a cubic phase.

During the first 1000 hours at 1000°C, the rate of degradation was much lower in 7.9YSZ2Mn than 7.9YSZ and 7.9YSZ1Mn (Fig. 6a), after this, however, it increased. The ageing also caused a visible change in the microstructure of the material; the grain boundary regions were depleted in Mn and the weak diffraction spots that are forbidden for the fcc phase were stronger in SADPs from the boundary region than from the grain interior (Fig. 10). The lower symmetry phase has grown in the grain boundary region (Fig. 11), demonstrating that cation diffusion also takes place in 7.9YSZ2Mn during the ageing at 1000°C. How cation diffusion in the 3-component system of 7.9YSZ2Mn causes an overall increase in lattice parameter during ageing is impossible to discuss from the present results because it is not known how Mn and Y are distributed among the various phases. EDS-analyses in the grain boundary regions were not obtained from single phased material because the smallest obtainable spot size in the TEM was too large to probe the grain boundary phase alone. The Y_2O_3/ZrO_2 ratio is the same in the grain boundaries and in the grains; therefore the high Y_2O_3/Mn_3O_4-ratio in the grain boundaries may be due to the presence of a low symmetry phase with a low Mn content. The diffusion processes which cause a separation of crystalline phases in the outer 50–100 nm of the grains may explain the faster degradation of 7.9YSZ2Mn which started after approximately 800 hours of ageing at 1000°C (Fig. 6a).

The conductivity degradation of 7.9YSZ1Mn is very similar to that of 7.9YSZ, indicating that doping with 1 mol% Mn is insufficient to stabilise the cubic structure. The degradation of the 7.9YSZ2Mn specimen first occurs at a lower rate than that in 7.9YSZ and 7.9YSZ1Mn, suggesting at first glance that the Mn doping stabilises the cubic phase and, thereby, the conductivity. However, after about 800 hours, the decrease in conductivity resembles that of the samples with less

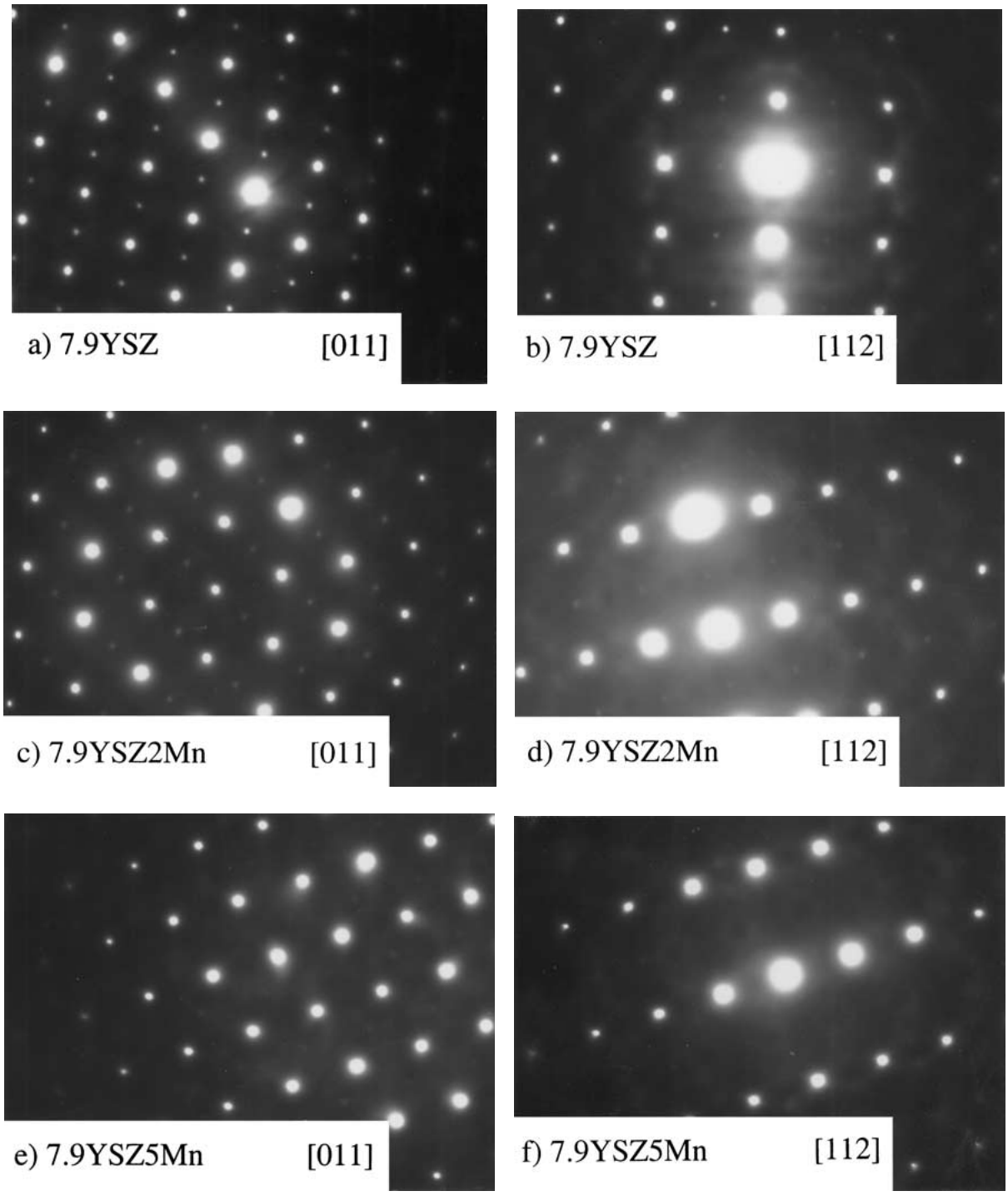

Figure 9 Selected area diffraction patterns for pure Mn-doped 7.9YSZ aged at 1000°C for 1000 hours. The relative intensity of the forbidden reflections is seen to decrease with increasing Mn content. No significant differences between these SADPs and those obtained from as-prepared samples are apparent. (a) 7.9YSZ along [011] (b) 7.9YSZ along [112] (c) 7.9YSZ2Mn along [011] (d) 7.9YSZ2Mn along [112] (e) 7.9YSZ5Mn along [011] (f) 7.9YSZ5Mn along [112].

Mn doping possibly due to growth of the low symmetry phase in the grain boundaries (Fig. 11), as suggested above. 7.9YSZ5Mn showed hardly any change in lattice parameter with ageing at 1000°C, the SADPs showed no indications of formation of tetragonal phase during the first 1000 hours and the conductivity showed no degradation during the ageing period of 2000 h. These three observations show clearly that 7.9YSZ5Mn is in the fully stabilised cubic phase field at 1000°C. As mentioned earlier, 7.9YSZ5Mn is fully stabilised at 1000°C (Fig. 9e and f) and, therefore, there are no phases to cause inhomogeneous distribution of the cations around the grain boundaries.

The diffusion coefficient of Mn in YSZ has been determined for both single crystal and polycrystalline materials [21]. Extrapolating their single crystal data to 1000°C, the diffusion coefficient of Mn gives a value of about 2×10^{-19} cm^2s^{-1}; the calculated diffusion length after a period of 800 hours is 10 nm. For the 7.9YSZ2Mn sample, a region of the order of 10 nm could thereby be expected to be depleted in Mn, which will then result in a lower degree of stability

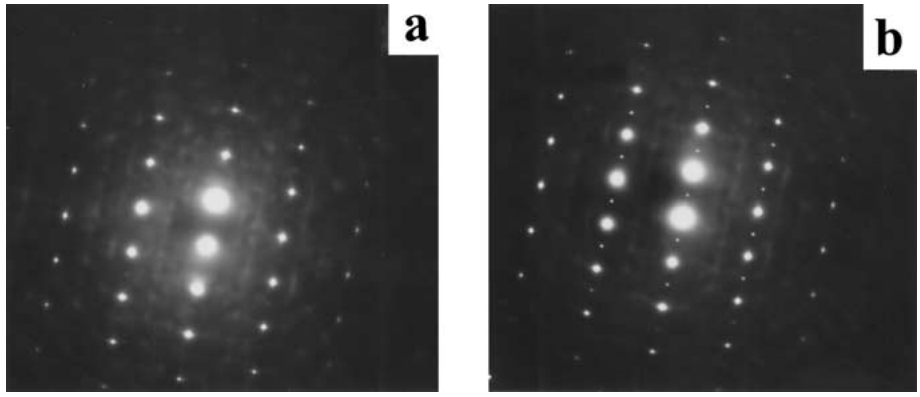

Figure 10 SADPs obtained with beam direction [013] of 7.9YSZ2Mn aged at 1000°C for 2000 hours. (a) The SADP is from the centre of a grain where no forbidden reflections are observed (b) The SADP is from an area close to a grain boundary where forbidden reflections are observed at {100}.

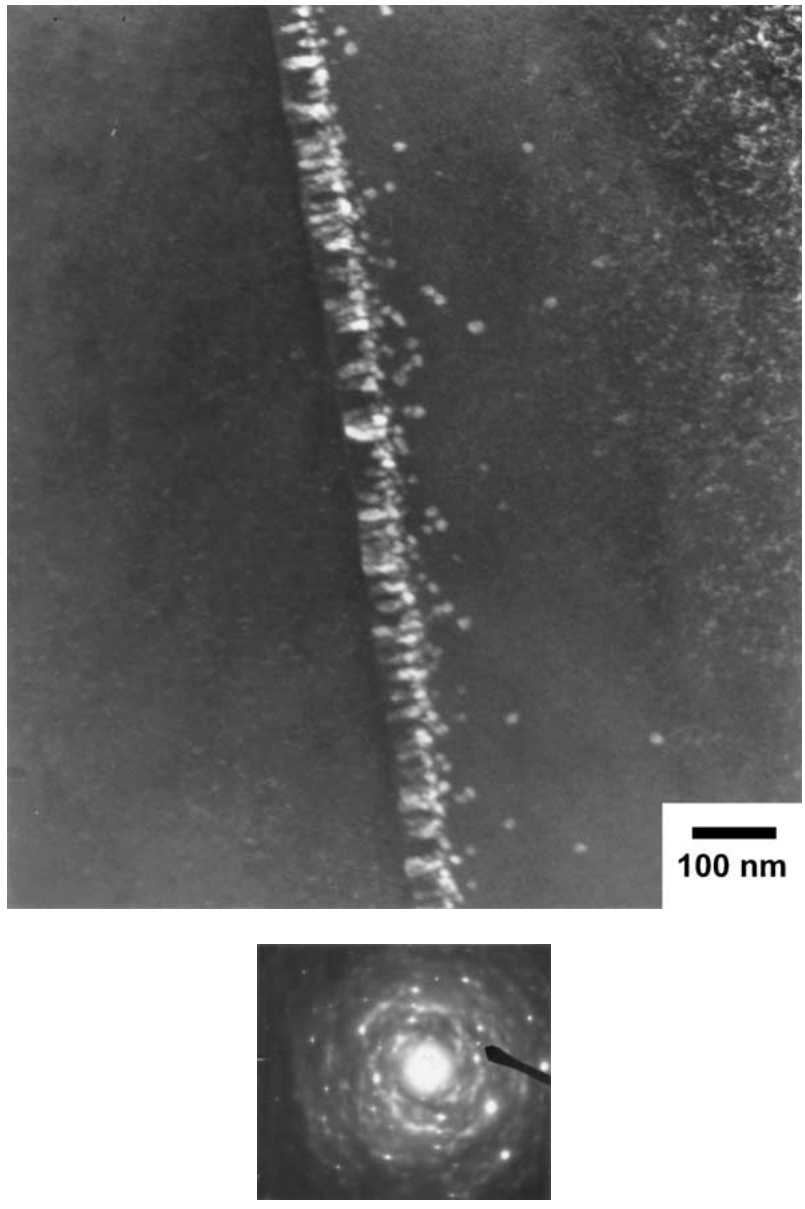

Figure 11 Dark field imaging of the grain boundary region of 7.9YSZ2Mn aged for 2000 hours. The extra spots are produced by a concentration of crystallites in a grain boundary region of width 50–100 nm. The diffracted beam used for the image is shown in the SADP.

of the cubic phase. This is in fair accordance with the observation of a region rich in the low symmetry phase at the grain boundary of the 7.9YSZ2Mn [22]. At 850°C the conductivity decreases with time for all compositions (Fig. 6b) due to loss of stabilisation of the cubic phase. At this temperature the diffusion of Mn is very slow, i.e. the degradation of the conductivity with time is an effect of the lack of stabilisation of the cubic phase for all compositions, hence also for 7.9YSZ5Mn. At the same time the conductivity at

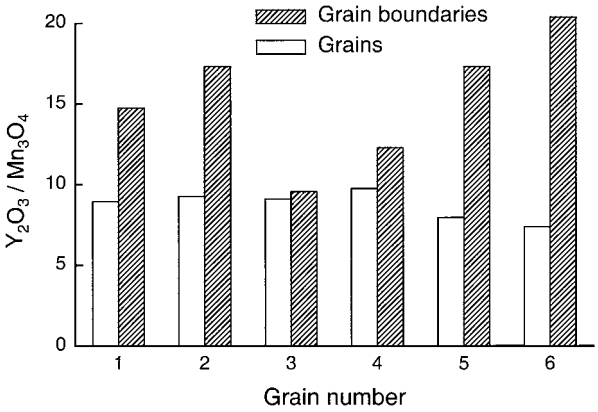

Figure 12 EDS-analyses of 7.9YSZ2Mn aged for 2000 hours in the centre of grains and in grain boundary regions, i.e. the region of the crystallites shown in Fig. 11. The high Y_2O_3/Mn_3O_4 ratio in these regions, as compared to the grain centres, reveals the depletion of Mn. Note that the Y_2O_3/ZrO_2-ratio is the same in the grain boundary regions and in the grains.

850°C is seen to be strongly influenced by doping with Mn.

Addition of Mn to YSZ clearly cannot be recommended as a means of improving its conductivity for the SOFC electrolyte. However, there may be other benefits that outweigh the lowering of conductivity, such as enhanced sintering, or the reduction of internal stress, given that some diffusion of Mn into YSZ from SOFC cathode material during device fabrication, sintering and operation is inevitable.

5. Conclusions

Addition of Mn to 7.9YSZ has been shown to decrease the initial oxide ion conductivity. This effect becomes more significant when lowering the temperature from 1000°C to 850°C. The addition of Mn is, at 1000°C, found to have a stabilising effect on 7.9YSZ for a Mn content above about 2 mol%. For lower Mn content no stabilisation effect is found at this temperature. At 850°C up to 5 mol% of Mn in 7.9YSZ is not found to stabilise the conductivity, but instead the Mn addition is only detrimental for the overall conductivity. These findings are important in SOFC development, especially considering current efforts to lower the operating temperature. It is clear from these investigations that Mn in YSZ should be avoided for low-temperature SOFCs. For high-temperature SOFCs, i.e. those operating at about 1000°C, a Mn content in the region 0.5–2 mol% should be avoided, as this will reduce the conductivity without providing a stabilisation of the conductivity. In the latter case, and where Mn diffusion from the cathode to the electrolyte cannot be avoided a Mn doping of approximately 5 mol% could be recommended to prevent degradation of the oxide ion conductivity.

6. Acknowledgements

The work has in part been supported through the Joule/Thermie project IDUSOFC (contract JOE3-CT-0005) under the European Commission. C. C. Appel publishes with the permission of the Geological Survey of Denmark and Greenland.

References

1. N. Q. MINH, *J. Amer. Ceram. Soc.* **76** (1993) 563.
2. S. P. S. BADWAL, *Solid State Ionics* **52** (1992) 23.
3. M. YOSHIMURA, *Ceramic Bull.* **67** (1988) 1950.
4. I. R. GIBSON, G. P. DRANSFIELD and J. T. S. IRVINE, *J. Eur. Ceram. Soc.* **18** (1998) 661.
5. T. KAWADA, N. SAKAI, H. YOKOKAWA and M. DOKIYA, *Solid State Ionics* **53–56** (1992) 418.
6. C. C APPEL, *Ionics* **1** (1995) 406.
7. C. C. APPEL, G. A. BOTTON, A. HORSEWELL and W. M. STOBBS, *J. Amer. Ceram. Soc.* **82** (1999) 429.
8. K. SASAKI, P. MURUGARAJ, M. HASEIDL and J. MAIER, in Proceedings of the 5th International Symposium on Solid Oxide Fuel Cells (SOFC-V), Aachen, edited by U. Stimming, S. C. Singhal, H. Tagawa and W. Lehnert (The Electrochemical Society, Pennington, 1997) Vol. 97-40, p. 1190.
9. C. CLAUSEN, C. BAGGER, J. B. BILDE-SØRENSEN and A. HORSEWELL, *Solid State Ionics* **70/71** (1994) 59.
10. F. W. POULSEN, J. J. BENTZEN and J. B. BILDE-SØRENSEN, in Proceedings of SOFC-Nagoya, International Symposium on Solid Oxide Fuel Cells, 13–14 November 1989 (SOFC Society of Japan, 1989) p. 93.
11. B. A. BOUKAMP, Equivalent Circuit, University of Twente, the Netherlands (1989).
12. L. J. VAN DER PAUW, *Philips Res. Repts.* **13** (1958) 1.
13. F. W. POULSEN, P. BUITINK and B. MALMGREN-HANSEN, in Proceedings of the 2nd International Symposium on Solid Oxide Fuel Cells (SOFC-II), Athens, 1991, edited by F. Grosz, P. Zegers, S. C. Singhal and O. Yamamoto (Office for Official Publications of the European Communities, Brussels, 1991) p. 755.
14. N. BONANOS, R. K. SLOTWINSKI, J. DRENNAN, P. BUTLER and B. C. H. STEELE, *Silicates Industriels* **9–10** (1985) 127.
15. N. BONANOS, B. C. H. STEELE and E. P. BUTLER, In "Impedance Spectroscopy" edited by J. Ross Macdonald (J. Wiley & Sons, New York, 1987) p. 225.
16. R. P. INGEL and D. LEWIS III, *J. Amer. Ceram. Soc.* **69** (1986) 325.
17. D.-J. KIM, *ibid.* **72** (1989) 1415.
18. A. KUZJUKEVICS and S. LINDEROTH, *Solid State Ionics* **92** (1996) 253.
19. Y. ZHOU, T.-C. LEI and T. SAKUMA, *J. Amer. Ceram. Soc.* **74** (1991) 633.
20. K. J. MCCLELLAN, S.-Q. XIAO, K. P. D. LAGERLOF and A. H. HEUER, *Phil. Mag. A* **70** (1994) 185.
21. D. WALLER, J. D. SIRMAN and J. A. KILNER, in Proceedings of the 5th International Symposium on Solid Oxide Fuel Cells (SOFC-V), Aachen, edited by U. Stimming, S. C. Singhal, H. Tagawa and W. Lehnert (The Electrochemical Society, Pennington, 1997) Vol. 97-40, p. 1140.
22. J. H. KIM and G. M. CHOI, *Solid State Ionics* **130** (2000) 157.

Received 24 May 2000
and accepted 7 May 2001